*EVS30 Symposium*
*Stuttgart, Germany, October 9 - 11, 2016*

# Investigations on a Hybrid Energy Storage System for an All-wheel Driven Motorcycle

Matthias Baumann[1], Michael Buchholz[1], Klaus Dietmayer[1]
[1]*Universität Ulm, Institut für Mess-, Regel- und Mikrotechnik, Albert-Einstein-Allee 41, 89081 Ulm,*
{*matthias.baumann, michael.buchholz, klaus.dietmayer*}*@uni-ulm.de*

**Abstract**

This paper presents a Hybrid Energy Storage System (HESS) for an all-wheel driven electric motorcycle. The HESS combines the standard battery of the vehicle, which only allows for very limited charging currents but has a high energy density, and a supercapacitor module, adding the possibility of high currents and therefore high power, but shows only limited energy storage abilities. For the HESS components, mathematical models have been retrieved from measurements of the battery cells and supercapacitors within a battery cell test rig. Based on this models, a non-linear observer is implemented, which allows to track the HESS states during operation on-board the vehicle. This state estimation is integrated within the real-time optimal control strategy based on a Model Predictive Control (MPC), allowing for an energy efficient operation of the overall system.

***Keywords:*** *battery, battery management, control system, optimization, supercapacitor*

## 1 Introduction

Hybrid Energy Storage Systems (HESS) combine the benefits of at least two energy storage components, e.g. one with high energy density and one with high power density. In the context of this paper, the HESS consists of a battery and a supercapacitor module (SC). The SC is integrated to protect the battery from peak loads and even allow for higher maximum recuperative currents, which enhances the battery's life time as well as the energy efficiency and, thus, leads to monetary savings.
Focus of this paper is a specific HESS for the all-wheel driven motorcycle shown in Fig. 1a, which was firstly presented in [2]. Compared to the commercially available vehicle [5] used as a basis, an additional hub motor enables a front-wheel drive. Since braking forces between front and rear wheel are usually distributed around a 70-80% to 30-20% ratio for two-wheelers, the front wheel is required to enable recuperation possibility in a relevant manner. So far, only a passive HESS was integrated in the vehicle for overall system's simplicity reasons. Since the built-in battery only allows for very limited charging currents, the HESS is required for efficient recuperation. However, the theoretical study [3] demonstrates the additional advantages of an active HESS, e.g. a higher utilization of the supercapacitors' voltage range, which leads to an higher energy storage capacity. Therefore, an active HESS architecture based on a model of the real HESS components is investigated in this paper. Fig. 1b presents the architecture

(a) All-wheel driven motorcycle.

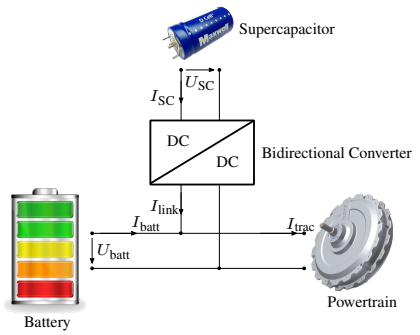


(b) Architecture of the HESS under investigation.

Figure 1: Considered system.

of the considered active HESS. The battery is directly connected to the powertrain and the SC module is placed in parallel with the help of a bidirectional converter.
This paper is structured as follows: Section 2 presents the modeling of the HESS components and the identification of their parameters as well as an observation to account for modeling errors. Section 3 depicts the control strategy based on a real-time capable solution of an optimal control problem. The obtained results are demonstrated in Section 4. In Section 5, the paper closes with a summery and an outlook on future work.

## 2 Modeling and State Observation

In this section, the mathematical model of the HESS is presented. The detailed derivation is shown in [3]. Afterwards, the results of the parameter identification are demonstrated. This section closes with the state observation using Kalman filtering to manage possible model inaccuracies.

### 2.1 HESS modeling

Fig. 2 shows the used equivalent circuits of the battery and the supercapacitor.

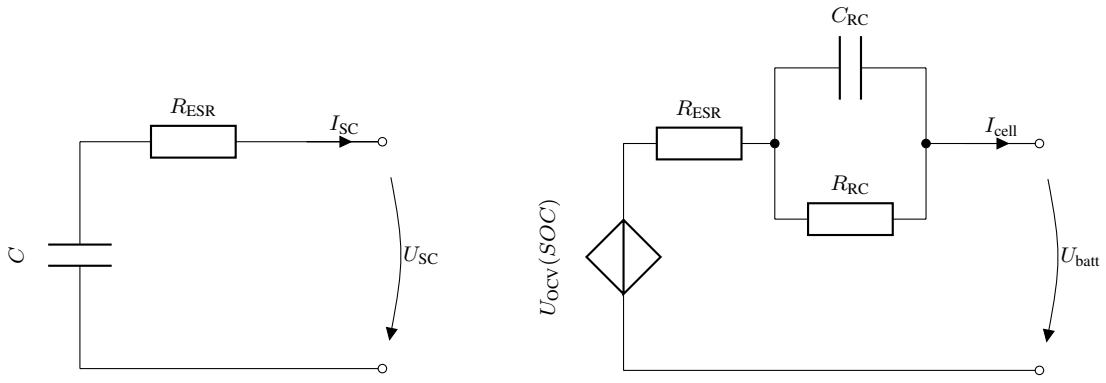


(a) Equivalent circuit of a supercapacitor.

(b) Equivalent circuit of a battery cell.

Figure 2: System models.

### 2.1.1 Supercapacitor

The entire supercapacitor module is obtained by a serial interconnection of individual cells. $N_{\text{cap}}$ defines the number of supercapacitor cells. One cell contains a capacity and an equivalent series resistance (see Fig. 2a). The dynamic behavior of the voltage of the capacity is described with the following ODE:

$$\dot{U}_C = \frac{1}{C} I_{\text{SC}}. \tag{1}$$

Using this, the voltage of the entire supercapacitor is defined as

$$U_{\text{sc}} = N_{\text{cap}}(U_C - R_{\text{ESR}} I_{\text{sc}}). \tag{2}$$

### 2.1.2 DC/DC Converter

Due to the fast time constants of the bidirectional DC/DC converter, the modeling is based on the power throughput. The converter delivers current according to an external set point. Quadratically losses depending on the supercapacitor's current $I_{\text{SC}}$ are assumed.
The resulting power at the battery/powertrain side can be calculated as follows:

$$P_{\text{link}} = U_{\text{sc}} I_{\text{sc}} - R_{\text{loss}} I_{\text{sc}}^2. \tag{3}$$

The sign of $I_{\text{SC}}$ specifies the direction of the energy/power flow in/out of the supercapacitor.

### 2.1.3 Battery

In Fig. 2b, the equivalent circuit of one battery cell is shown. It contains a voltage supply depended on the actual state of charge ($SOC$) of the cell, an equivalent series resistance and, for its dynamic behavior, an RC element. The entire battery consists of $N_{\text{s}}$ serial interconnected battery bricks, where each brick contains $N_{\text{p}}$ parallely interconnected battery cells.
The change of the $SOC$ can be written as

$$\dot{SOC}_{\text{batt}} = -\frac{I_{\text{batt}}}{N_{\text{p}} C_{\text{batt}}}, \tag{4}$$

where $C_{\text{batt}}$ is the nominal battery capacity of the cell.
With the use of Kirchhoff's laws, the current of the battery is defined as

$$I_{\text{batt}} = \frac{P_{\text{trac}} - P_{\text{link}}}{U_{\text{batt}}}. \tag{5}$$

Using $I_{\text{batt}} = N_{\text{p}} I_{\text{cell}}$, the overall battery voltage is given by

$$U_{\text{batt}} = N_{\text{s}} \left( U_{\text{OCV}}(SOC_{\text{batt}}) - U_{\text{RC}} - \frac{R_{\text{ESR}}}{N_{\text{p}}} I_{\text{batt}} \right). \tag{6}$$

Inserting Eq. (6) into Eq. (5) and solcing for $I_{\text{batt}}$ yields a quadratic equation for $I_{\text{batt}}$. The resulting physically valid solution of the battery current is

$$\begin{aligned} I_{\text{batt}} = {} & \frac{-N_{\text{s}} N_{\text{p}} \big(U_{\text{OCV}}(SOC_{\text{batt}}) - U_{\text{RC}}\big)}{-2\, N_{\text{s}}\, R_{\text{ESR}}} \\ & + \frac{\sqrt{\Big(N_{\text{s}} N_{\text{p}} \big(U_{\text{OCV}}(SOC_{\text{batt}}) - U_{\text{RC}}\big)\Big)^2 + 4\, N_{\text{s}} N_{\text{p}}\, R_{\text{ESR}} ((U_{\text{sc}}\, I_{\text{sc}} - R_{\text{loss}}\, I_{\text{sc}}^2) - P_{\text{trac}})}}{-2\, N_{\text{s}}\, R_{\text{ESR}}}. \end{aligned} \tag{7}$$


(a) Cell tester.

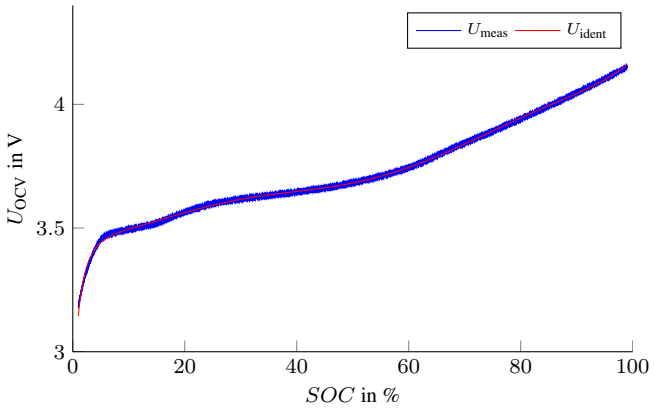


(b) Open-circuit voltage in function of the battery's $SOC$.

Figure 3: Test rig and measured data.

Thuis battery current can then be inserted into the ODE of the RC circuit, which is given by

$$\dot{U}_{\text{RC}} = -\frac{1}{R_{\text{RC}}\, C_{\text{RC}}}\, U_{\text{RC}} + \frac{1}{C_{\text{RC}}\, N_{\text{p}}}\, I_{\text{batt}}. \tag{8}$$

### 2.1.4 Overall Model

Using the states $\boldsymbol{x} = [U_{\text{C}},\, U_{\text{RC}},\, SOC_{\text{batt}}]^{\text{T}}$, the input $u = I_{\text{SC}}$, and the deterministic disturbance $z = P_{\text{trac}}$ induced by the powertrain, the overall nonlinear model of the HESS can be written in the follwing state-space form:

$$\dot{\boldsymbol{x}} = \boldsymbol{f}(\boldsymbol{x},\, u,\, z). \tag{9}$$

The system outputs $\boldsymbol{y} = [I_{\text{batt}},\, U_{\text{batt}},\, U_{\text{SC}}]^{\text{T}}$ are then given by

$$\boldsymbol{y} = \boldsymbol{g}(\boldsymbol{x},\, u,\, z). \tag{10}$$

## 2.2 Parameter Identification

So far, only the model structures of the energy storage components, i.e. the model equations of battery and SC, have been derived, their parameters are still unknown. Since the models comprise simplifications and the parameters are not known from physical or chemical considerations, they are retrieved from measurement data by identification means. The identification data was recorded using the cell tester shown in Fig. 3a.

First, the open circuit voltage of the battery depending on the actual state of charge is characterized. Therefore, a discharge of fully charged cells with $0.1$ C-rate was done. The results are shown in Fig. 3b. The identified nonlinear function (red line) matches the measured data (blue line) very accurately, which is also visible from the root mean squared error of $4.4\,\text{mV}$.

In Fig. 4, the identification results of the battery cell are presented. The upper plot shows the used current profile. In the lower plot, the measured (blue line) as well as the simulated voltage (red line) using Eq. 6 with the identified parameters are presented. With a root mean squared error of $3.6\,\text{mV}$, the accuracy of the model is very good.

Finally, the identification results of the supercapacitors' model are depicted in Fig. 5. Identically to the battery's identification figure, the upper plot contains the current and the lower plot the identification results. The root mean squared error for the supercapacitors' voltage is $5.0\,\text{mV}$ and thus also very good.

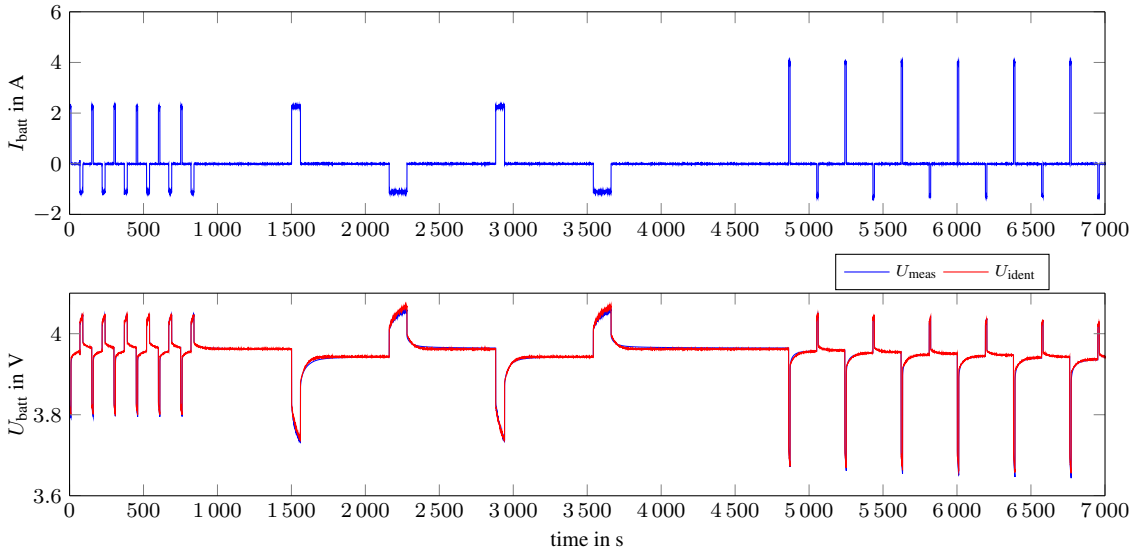


Figure 4: Identification results of a battery cell.

## 2.3 State Observation

To compensate for any possible model inaccuracies, an Unscented Kalman Filter (UKF) is used. An UKF is a nonlinear version of the classical Kalman filter, which is able to handle the model nonlinearities comprised in the derived model equations in a accurate and numerically efficient manner (see e.g. [6]). Fig. 6 clarifies the advantage of the used UKF. For this example, the model parameters are deliberately falsified. The green line shows the states just using the model equations (open-loop/feed-forward simulation). This leads to deviations of the actual values (red line). The blue line shows the states ($U_{\mathrm{C}}$, $U_{\mathrm{RC}}$) using the UKF comprising the same falsified model. Despite the incorrect model parameters, the UKF yields very good results due to its internal feed-back structure.

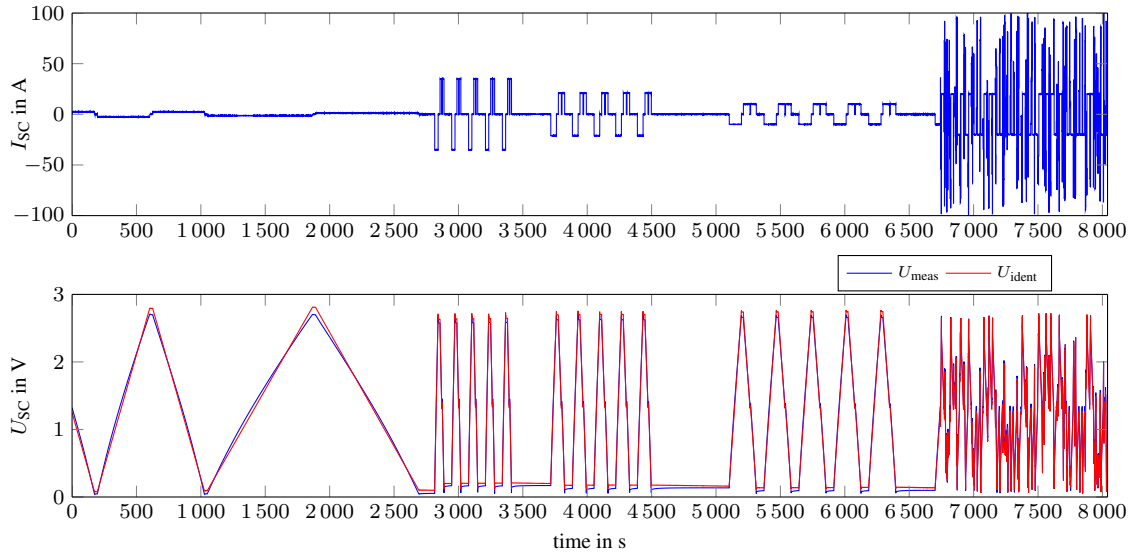


Figure 5: Identification results of a supercapacitor cell.

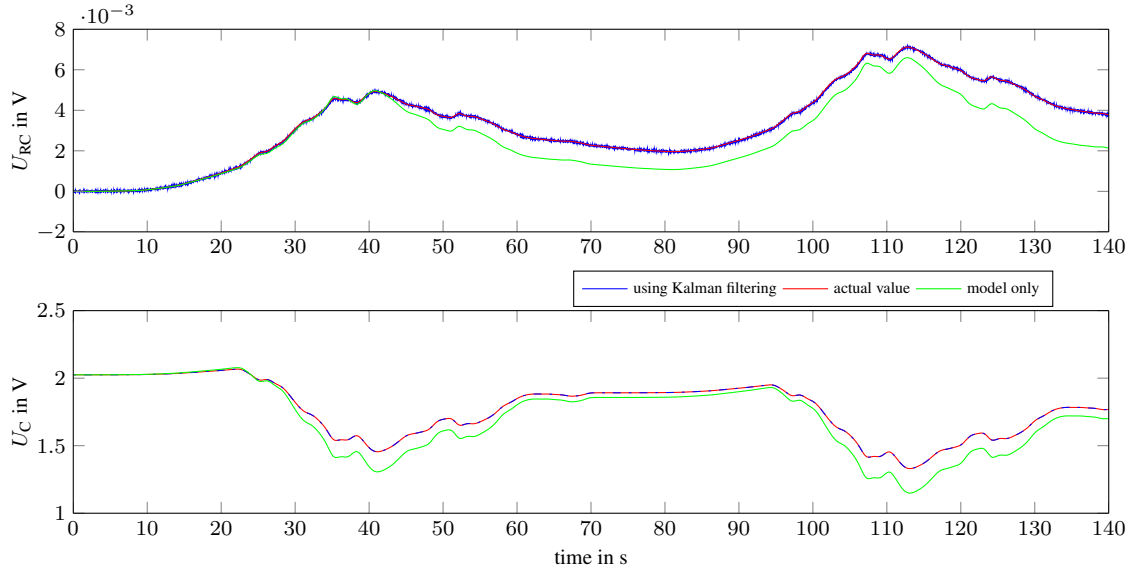


Figure 6: UKF example to show advantages of filtering vs. simulation.

## 3 Control Strategy

The control strategy of the active HESS is based on solving an optimal control problem (cp. [3]) in real-time to enable on-board the vehicle application. This is done over an receding prediction horizon in each sample time step of the algorithm. The disturbance $z$ is assumed to be predictable over the prediction horizon. This could be achieved for example with the help of map information, a defined route or estimation methods. Due to the insignificant change of $SOC_{\mathrm{batt}}$ due to its very slow dynamics compared to the voltages of the capacitors, it is assumed to be stepwise constant. This means that is is kept constant within the prediction horizon in the following optimization algorithm, but updated every time step the algorithm is re-started.
The main goal of the HESS is to protect the battery from damaging current with the help of the super-capacitor module. This also leads to a positive effect on the battery's lifetime. Therfore, the following optimal control problem (OCP)

$$\begin{aligned} \min_{\bar{u}(t)} \quad & J(\boldsymbol{x}_k, \bar{u}) = \int_{t_k}^{t_k+T} l(\bar{\boldsymbol{x}}(t), \bar{u}(t), \bar{z}(t))\ \mathrm{d}t \\ s.t. \quad & \dot{\bar{\boldsymbol{x}}}(t) = \boldsymbol{f}(\bar{\boldsymbol{x}}, \bar{u}, \bar{z}), \bar{\boldsymbol{x}}(t_k) = \boldsymbol{x}_k, \\ & \bar{u}(t) \in [I_{\mathrm{SC}}^-, I_{\mathrm{SC}}^+]\,, \end{aligned} \tag{11}$$

has to be solved on-line, where $t_k$ is the sample time at which the OCP is solved starting from $\boldsymbol{x}_k = \boldsymbol{x}(t_k)$, $T$ is the prediction horizon, and the variables with the over-set bar are the predicted quantities. The integral costs $l(\bar{\boldsymbol{x}}(t), \bar{u}(t), \bar{z}(t))$ of the OCP are:

$$\begin{aligned} l(\boldsymbol{x},\, u,\, z) = {} & \gamma_1 I_{\mathrm{batt}}^2 + \gamma_2 \big( (R_{\mathrm{loss}} + N_{\mathrm{cap}}\, R_{\mathrm{ESR,cap}}) u^2 + R_{\mathrm{ESR,batt}}\, I_{\mathrm{batt}}^2 \big) \\ & + \gamma_3 f_{\mathrm{pen}}(SOC_{\mathrm{batt}}, SOC_{\mathrm{batt}}^+, SOC_{\mathrm{batt}}^-) + \gamma_4 f_{\mathrm{pen}}(U_{\mathrm{SC}}, U_{\mathrm{SC}}^+, U_{\mathrm{SC}}^-) \\ & + \gamma_5 f_{\mathrm{pen}}(I_{\mathrm{batt}}, I_{\mathrm{batt}}^+, I_{\mathrm{batt}}^-) + R u^2 + \boldsymbol{x}_{\boldsymbol{\delta}}{}^{\mathrm{T}} \boldsymbol{Q} \boldsymbol{x}_{\boldsymbol{\delta}} \end{aligned} \tag{12}$$

$\gamma_1$ and $\gamma_2$ are weighting factors to protect the battery from peak currents and to minimize ohmic losses, respectively. For the state-depended variables $SOC_{\mathrm{batt}}$, $U_{\mathrm{SC}}$, $I_{\mathrm{batt}}$, differentiable penalty functions are used, which are weighted with $\gamma_3$, $\gamma_4$ and $\gamma_5$, respectively. The penalty functions are zero if the variable is within the respective limits and increase quadratically beyond the limits. These differentiable penalty

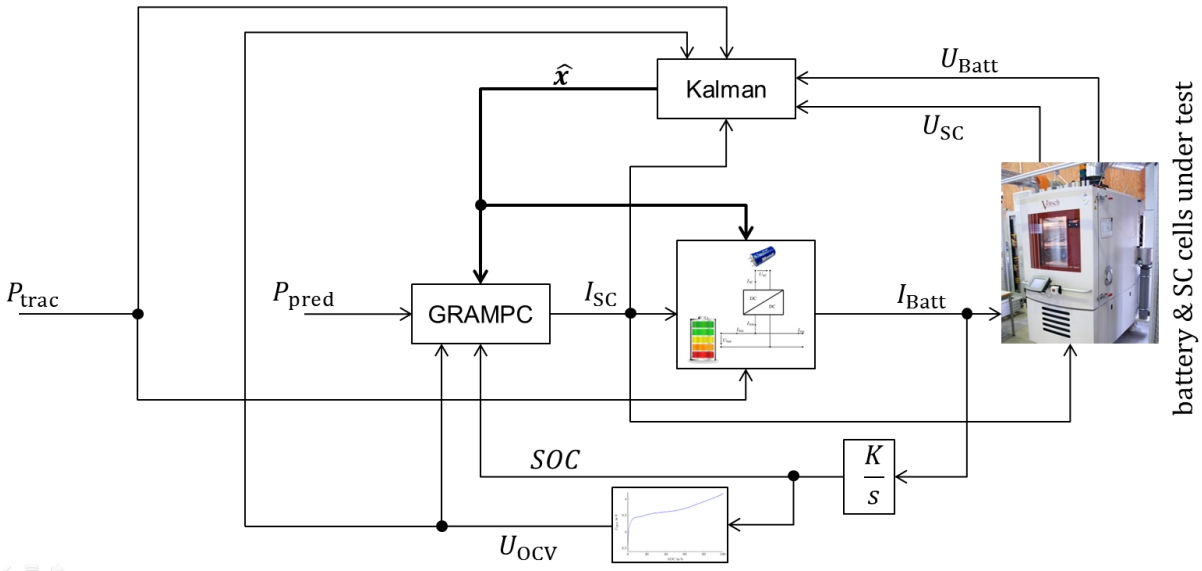


Figure 7: Simulation setup.

functions are introduced and applied instead of hard constraints for numerical efficiency reasons. With the factor $R$, the use of the input is penalized. Using $\boldsymbol{x}_\delta = \boldsymbol{x} - \hat{\boldsymbol{x}}$ the matrix $\boldsymbol{Q}$ weights the deviation to a given target state $\hat{\boldsymbol{x}}$. With the ratio of the weighting factors, the optimal compromise between the different goals can be adjusted.

The OCP is solved online based on the open-source software GRAMPC [7] (available at `http://sourceforge.net/projects/grampc/`). GRAMPC uses a gradient-based method (see also [4]) with a finite number of iterations. this yields to possibly sub-optimal solutions the algorithm, but on the other side makes the algorithm real-time capable. Additionally, the convergence behavior of the presented method is strong, because it is an iterative algorithm, thus leading to close-to-optimum results of the OCP and therefore good control results for the HESS, as can be seen in the next section.

As a result of the optimization algorithm, the approximate optimal solutions for the given OCP $\bar{u}(t)$ and the associated $\bar{\boldsymbol{x}}(t)$ with $t \in [t_k,\, t_k + T]$ are retrieved in each time step. The first part of the control trajectory $\bar{u}(t)$ with $t \in [t_k,\, t_k + \Delta t]$ is applied as control input. In the next sampling step $t_{k+1} = t_k + \Delta t$, the OCP is solved again with the new initial state $\bar{\boldsymbol{x}}_{k+1}$ and using the previous optimal solution as a starting point.

# 4 Results

To verify the functionality of the proposed HESS and dedicated control strategy, experimental investigations have been performed. The converter is simulated in software and individual battery cells and supercapacitors representing the entire HESS are integrated in a battery test rig. Fig. 7 demonstrates the overall test set-up. Within the optimization algorithm, the supercapacitors' current is calculated depending on the power demand. Using the derived model, the battery's current results. The test rig adjusts these currents to the real cells (battery and SC). This leads to voltage responses, which can be used for the state observation as described in Section 2. The state of charge of the battery is calculated using Coulomb counting. Then, SOC can be used to determine the open circuit voltage within the battery model, which is part of the optimization algorithm.

The tested power profile is derived from the velocity profile of the urban part of the ARTEMIS cycle (see [1]). The battery limits are between $-10$ A and 50 A and the limits of the supercapacitor module are $-100$ A and 100 A. Fig. 8 shows the results of this experiment. The upper plot is the demanded power profile, which is above the possibilities of the battery. In the middle plot, the currents are presented.

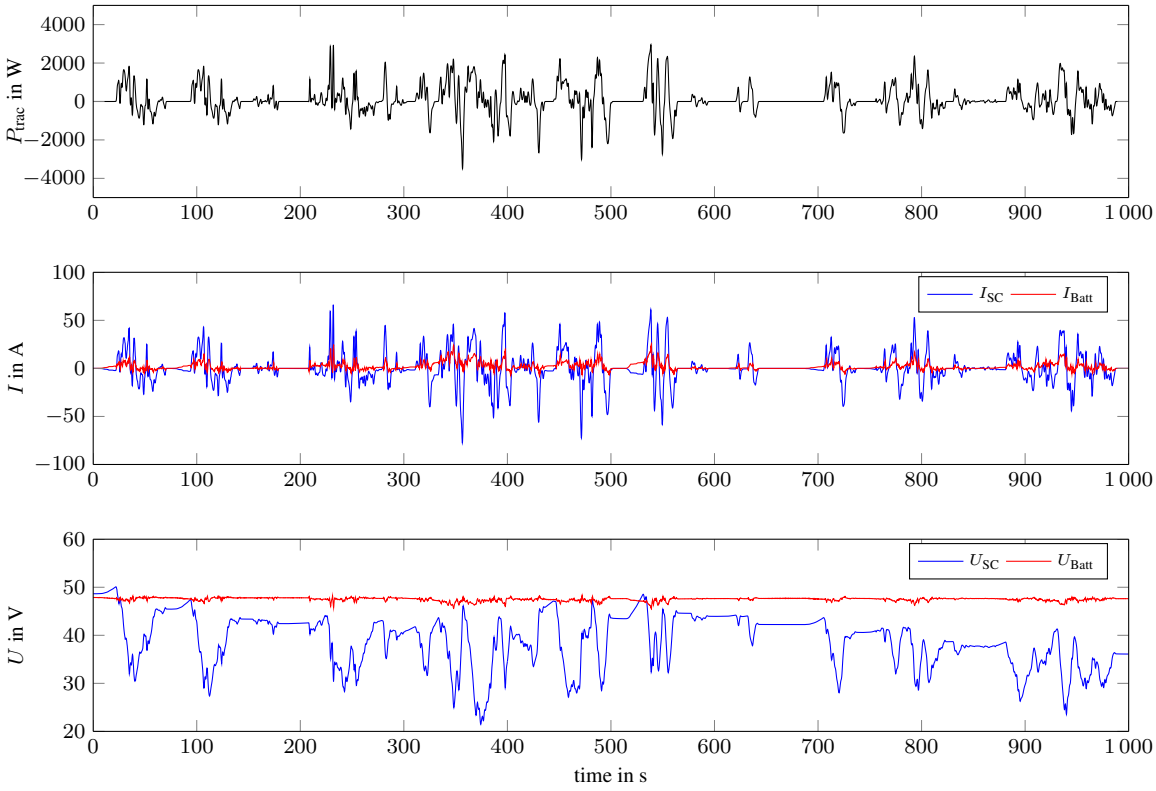


Figure 8: Experimental results.

The currents stay within the given limits during the whole profile by virtue of the control strategy. The voltages are shown in the lower plot. The battery's voltage is almost constant due to its high energy capacity, while the supercapacitors' voltage varies between 20 V and 50 V. Thus, thanks to the HESS, it is possible to mange a power profile which is above the given battery limits while saving the battery from damaging peak currents. The load prediction is used to transfer energy between the SC and the battery to guarantee the supercapacitors' support if it is needed. The optimization horizon is chosen to 20 s with a sampling rate of 200 ms. The OCP is solved on the real-time hardware MircoLabBox in 1.5 ms, which is far below the sampling rate. Therefore, the proposed algorithm can definitely be considered real-time capable even for less powerful ECUs. Overall, such a system enhances the lifetime of a battery while even improving the performance and dynamics of the overall energy system.

# 5 Conclusion

In this contribution, a model predictive control strategy for a semi-active HESS was presented. First, the needed model equations were derived. Subsequently, the parameters of the HESS model were identified based on measured data of the components. For a robust operation, an Unscented Kalman Filter (UKF) was introduced, which observes the state variables. Afterwards, the functionality of the developed algorithm was validated with experimental measurements on a test rig. Therefore, a power profile based on the ARTEMIS drive cycle was tracked. The experimental results show that with the use of the HESS, the battery is protected from high and damaging currents. Simultaneously, sufficient power is delivered. In further work, ist is planned to integrate the active HESS in the all-wheel driven motorcycle to conduct driving tests.

## Acknowledgments

The authors would like to thank the Ministry of Economic Affairs, Labour and Housing of Baden-Württemberg, as well as the industry partners ID-BIKE GmbH, Stuttgart, Gigatronik Technologies GmbH, Ulm, ipdd GmbH & Co.KG, Stuttgart, for funding and supporting the development of the all-wheel driven electric motorcycle. The cell tester used in the work was financed by a grant from the Ministry of Science, Research and the Arts of Baden-Württemberg.

## References

[1] Michel André. The ARTEMIS european driving cycles for measuring car pollutant emissions. *Science of The Total Environment*, 2004.

[2] Matthias Baumann, Michael Buchholz, and Klaus Dietmayer. A two-wheel driven power train for improved safety and efficiency in electric motorbikes. In *Electric Vehicle Symposium (EVS 29)*, 2016.

[3] Matthias Baumann, Michael Buchholz, and Klaus Dietmayer. Model Predictive Control of a Hybrid Energy Storage System Using Load Prediction. In *International Conference on Control and Automation*, 2017.

[4] Knut Graichen and Bartosz Käpernick. A real-time gradient method for nonlinear model predictive control. In *Frontiers of Model Predictive Control*. 2012.

[5] ID-BIKE GmbH. Elmoto. `http://www.elmoto.com/de/products/hr2-evo/`, accessed on 2017-05-12.

[6] Simon J. Julier and Jeffrey K. Uhlmann. A new extension of the kalman filter to nonlinear systems. In *International Symposium on Aerospace/Defence Sensing, Simulation and Control*, 1997.

[7] Bartosz Käpernick and Knut Graichen. The gradient based nonlinear model predictive control software GRAMPC. In *European Control Conference (ECC)*, 2014.

## Authors

**Matthias Baumann, M.Sc.,** received his master's degree in Communications and Computer Engineering from Ulm University in 2013. Since 2013, he is a researcher at the Institute of Measurement, Control, and Microtechnology at Ulm University, working towards his Ph.D. degree in the field of Electric Mobility.

**Dr.-Ing. Michael Buchholz** received his diploma degree in Electrical Engineering and Information Technology as well as his Ph.D. degree from University of Karlsruhe/Karlsruhe Institute of Technology in 2004 and 2010, respectively. Since 2009, he has been serving as a group leader and lecturer at the Institute of Measurement, Control, and Microtechnology at Ulm University. His main research interests comprise system identification and diagnosis, electric mobility, automated and connected driving, and mechatronical systems.

**Prof. Dr.-Ing. Klaus Dietmayer** is director of the Institute of Measurement, Control, and Microtechnology at Ulm University and head of driveU. His main research interests are information fusion, classification methods, stochastic filters and tracking, signal processing, and dynamical modeling and control within automotive applications.